npj | Quantum Materials

www.nature.com/npjquantmats

ARTICLE OPEN

Check for updates

Giant Seebeck effect across the field-induced metal-insulator transition of InAs

Alexandre Jaoui[1,2✉], Gabriel Seyfarth[3,4], Carl Willem Rischau[2], Steffen Wiedmann[5,6], Siham Benhabib[3], Cyril Proust[3], Kamran Behnia[2] and Benoît Fauqué[1✉]

Lightly doped III–V semiconductor InAs is a dilute metal, which can be pushed beyond its extreme quantum limit upon the application of a modest magnetic field. In this regime, a Mott-Anderson metal–insulator transition, triggered by the magnetic field, leads to a depletion of carrier concentration by more than one order of magnitude. Here, we show that this transition is accompanied by a 200-fold enhancement of the Seebeck coefficient, which becomes as large as 11.3 mV K^{-1}≈ 130$\frac{k_B}{e}$ at $T = 8$ K and $B = 29$ T. We find that the magnitude of this signal depends on sample dimensions and conclude that it is caused by phonon drag, resulting from a large difference between the scattering time of phonons (which are almost ballistic) and electrons (which are almost localized in the insulating state). Our results reveal a path to distinguish between possible sources of large thermoelectric response in other low-density systems pushed beyond the quantum limit.

npj Quantum Materials (2020)5:94 ; https://doi.org/10.1038/s41535-020-00296-0

INTRODUCTION

The thermoelectrical properties of low carrier density metals are of fundamental and technological interest. Owing to their small Fermi temperatures (T_F), their diffusive Seebeck effect ($S_{xx} = \frac{E_x}{\Delta_x T}$) can be large and, as such, used to develop high-performance thermoelectric devices[1]. At low temperature, their thermoelectrical response is also a fine probe of their fundamental electronic properties, in particular in the presence of a magnetic field[2]. As an example, the large quantum oscillations observed in the Nernst effect ($S_{xy} = \frac{E_y}{|\Delta_x T|}$) of semimetals[3–5] or doped semiconductors[6–8] have been used to map out their Fermi surfaces and to reveal the Dirac/Weyl nature of the electronic spectrum of Bi[5], $Pb_{1-x}Sn_xSe$[7] or $ZrTe_5$[8].

For most dilute metals, a magnetic field of a few Tesla is enough to confine all the charge carriers in the lowest Landau level (LLL), the so-called quantum limit. At low temperature, this is concomitant with an increase of S_{xx} (and S_{xy})[7–10]. This increase can be found at higher temperatures, as illustrated by the large Seebeck effect recently observed in the quantum limit regime of the Weyl semimetal TaP[11] or in the fractional quantum Hall regime of two dimensional electron gas (2DEGs)[12]. In these systems, the amplitude of $\frac{S_{xx}}{T}$ is much larger than $\frac{k_B}{e}\frac{1}{T_F}$, the natural thermoelectric scale of the diffusive response. This surprisingly large S_{xx} can be either the result of an unbounded diffusive thermoelectric power specific to nodal metals[13] or to the coupling of electrons with the phonon bath. In the latter case, the so-called phonon drag, the amplitude of S_{xx} is dictated by the momentum transfer between the electron and phonon baths and can be much larger than $\frac{k_B}{e}$[14]. The phonon drag effect is well-known to enhance S_{xx} in low-doped semiconductors at zero magnetic field but also in the quantum limit regime[9,15]. Here, we present a study of the electrical and thermoelectrical properties of InAs, a bulk narrow-direct-gap semiconductor, beyond its quantum limit and up to a so-far unexplored range of temperature and magnetic field. Our findings show that the field induces a metal–insulator transition (MIT) that is accompanied by a giant peak in the Seebeck effect, as large as $S_{xx} = 11.3$ mV K^{-1} at $T = 8$ K. Based on a study of the thermal response as a function of sample dimensions, we argue that this giant Seebeck effect results from phonon drag. Our results demonstrate a new road to achieve large thermoelectric response that can be explored in other dilute metals recently identified.

RESULTS

A dilute metal at zero magnetic field

We show in Fig. 1 the temperature dependence of the resistivity (ρ_{xx}), the Seebeck coefficient (S_{xx}) and the thermal conductivity (κ) of an *n*-type InAs with a Hall carrier density $n_H = 2.0 \times 10^{16}$ cm^{-3}. The Fermi surface of InAs, studied by low magnetic field quantum oscillation measurements (see Supplementary Note 1), is formed by a single spherical pocket located at the Γ-point of the Brillouin zone with a carrier density $n_{SdH} = 1.6 \times 10^{16}$ cm^{-3} ($T_F = 100$ K) and mass carrier $m^* = 0.023m_0$. From room temperature down to T_F, ρ_{xx} is metallic and the non-degenerate electrons are mainly scattered by phonons. Below T_F, ρ_{xx} increases with decreasing temperature as electrons become more and more degenerate with a mobility limited by ionized-impurity scattering[16]. Below $T = 20$ K, ρ_{xx} is constant with a residual resistance of $\rho_0 = 12$ mΩ.cm and a Hall mobility $\mu_H = 24{,}000$ cm^2 V^{-1} s^{-1}. The electronic contribution (κ_{el}) to κ is given by the Wiedemann Franz law $\kappa_{el} = \frac{L_0 T}{\rho_0} = 0.19$ mW K^{-2} m^{-1}. It is much smaller than the κ shown in Fig. 1b) and points to a purely phononic origin to κ.

Below $T = 6$ K, κ scales with T^3. The phonon mean free path, ℓ_{ph}, can be estimated through the kinetic formula $\kappa = \frac{1}{3} C_{ph} v_{ph} \ell_{ph}$, where $C_{ph} = \beta_{ph} T^3$ is the specific heat associated with phonons at low

[1]JEIP, USR 3573 CNRS, Collège de France, PSL Research University, 11, Place Marcelin Berthelot, 75231 Paris, France. [2]Laboratoire de Physique et Etude des Matériaux (CNRS/UPMC), Ecole Supérieure de Physique et de Chimie Industrielles, 10 Rue Vauquelin, 75005 Paris, France. [3]Laboratoire National des Champs Magnétiques Intenses (LNCMI-EMFL), CNRS, UGA, UPS, INSA, Grenoble/Toulouse, France. [4]Université Grenoble-Alpes, Grenoble, France. [5]High Field Magnet Laboratory (HFML-EMFL), Radboud University, Toernooiveld 7, 6525 ED Nijmegen, The Netherlands. [6]Radboud University, Institute for Molecules and Materials, 6525 AJ Nijmegen, The Netherlands. ✉email: alexandre.jaoui@espci.fr; benoit.fauque@espci.fr

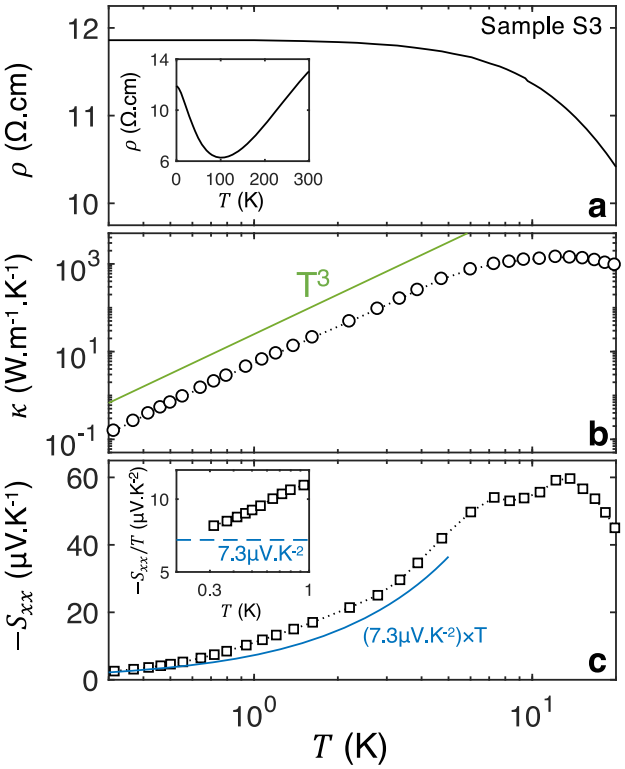

Fig. 1 Transport properties of n-type InAs at $B = 0$T. a Resistivity (ρ), **b** thermal conductivity (κ), and **c** $-S_{xx}$ of InAs sample S3 as functions of the temperature at $B = 0$T (see Supplementary Note 1). Inset in **a** shows ρ up to $T = 300$ K. The solid green line in **b** represents a T^3 power law characteristic of phonon contribution in the ballistic regime. The inset in **c** shows $-\frac{S_{xx}}{T}$ plotted as a function of the temperature in the sub-Kelvin region. The blue dashed line corresponds to the value $\frac{S_{xx}}{T} = 7.3\,\mu\text{V K}^{-2}$, which is expected in the diffusive regime of a degenerate electron gas with $T_F = 100$ K (see Supplementary Note 3). The diffusive contribution is further emphasized as a blue line in **c**).

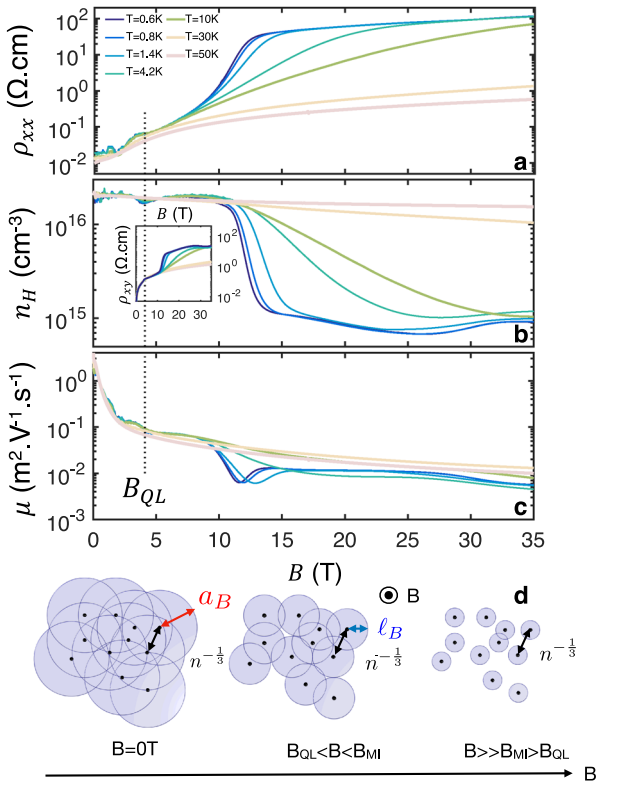

Fig. 2 Metal–Insulator transition in InAs. a Transverse ($\vec{j} \perp \vec{B}$) magnetoresistivity of sample S1 for various temperatures up to $B = 35$ T. The evolution of the Hall carrier concentration n_H with the magnetic field, for the same sample and temperatures, is featured in **b** alongside the electronic mobility μ in **c**. Inset of **b** shows the Hall resistivity of the sample. The vertical dotted line marks the quantum limit at B_{QL}. **d** Sketch of the magnetic freeze-out effect: as the magnetic field increases the effective Bohr radius $a_B^* = (a_{B,\perp}^2 a_{B,\parallel})^{\frac{1}{3}}$ (see the text for the definition) is decreased. When the overlap between the wave functions is sufficiently reduced, a metal–insulator transition is expected to occur at B_{MI} when the condition $n^{1/3}(a_B^*(B = B_{MI})) = \delta$ is satisfied where $\delta \approx 0.3$–0.4.

temperature with $\beta_{ph} = 3.68\,\text{J K}^{-4}\,\text{m}^{-3}$ (ref. [17]) and v_{ph} is the sound velocity $v_{ph} = 2.5$–$4.4\,\text{km s}^{-1}$ (ref. [18]). The deduced $\ell_{ph} \simeq 0.5$–1mm is comparable with the sample cross-section, $\bar{s} = \sqrt{(\omega t)} = 0.5$ for S3 (where ω and t are the sample width and thickness much shorter than its length, $L = 8$mm). Phonons are thus in the ballistic regime. Similarly to κ, S_{xx} peaks around $T = 10$K. In the zero temperature limit $\frac{S_{xx}}{T}$ saturates to a value of $7.8\,\mu\text{V K}^{-2}$, which is in quantitative agreement with the expected value for the diffusive response of a degenerate semiconductor in the ionized-impurity scattering regime (see Supplementary Note 3) . The finite-temperature extra contribution to S_{xx} comes from the phonon-drag effect. In summary, at zero magnetic field, InAs is a dilute metal with one electron per 10^6 atoms. The mobility of these carriers does not evolve much with cooling. Yet, it is high enough to allow the observation of quantum oscillations. Thermal transport is dominated by phonons, which become ballistic below $T = 10$ K while the thermoelectric response is purely diffusive in the zero temperature regime with a modest phonon drag component at finite temperature.

Field-induced metal–insulator transition in InAs

Let us now discuss the evolution in field of the electrical and thermoelectrical properties of InAs, which are shown respectively on Figs. 2 and 3. At low magnetic fields, ρ_{xx}, n_H, and S_{xx} display quantum oscillations. The last quantum oscillation occurs at $B = 4.1$ T (see Supplementary Note 1). This magnetic field is defined as B_{QL} above which all the carriers are confined in the lowest Landau level (LLL). Up to $B = 10$ T, ρ_{xx} and S_{xx} increase while n_H remains constant. From $B = 10$ T to $B = 15$ T, ρ_{xx} increases by about two orders of magnitude while n_H drops by a factor close to 20 and S_{xx} by a factor of three. This marks the entrance in the magnetic freeze-out regime, in good agreement with early measurements[19,20]. This regime has been thoroughly studied in the low-doped narrow gap semiconductors InSb and $Hg_{1-x}Cd_xTe$ ($n_H = 10^{-14}$–$10^{-15}\,\text{cm}^{-3}$)[21,22]. It was shown that the magnetic field induces a MIT ascribed as a magnetic field assisted Mott-Anderson transition in lightly doped semiconductors (see ref. [22] for a review). A sketch of this effect is shown in Fig. 2d). For $B > B_{QL}$, the in-plane electronic wave extension is equal to $a_\perp = 2\ell_B$ with $\ell_B = \sqrt{(\frac{\hbar}{eB})}$ and shrinks with the magnetic field. Parallel to the magnetic field the characteristic spatial extension is given by $a_{B,\parallel} = \frac{a_B}{\log(\gamma)}$, where $\gamma = (\frac{a_B}{l_B})^2$[23,24]. Once the overlap between the wave functions of electrons is sufficiently reduced, a MIT is expected to occur at $B = B_{MI}$, i.e., when:

$$n^{1/3}\left(a_{B,\perp}^2 a_{B,\parallel}\right)^{\frac{1}{3}} = \delta \quad (1)$$

with $\delta = 0.3$–0.4 for InSb and $Hg_{1-x}Cd_xTe$. The carrier dependences of B_{QL} and B_{MI} for these two systems are shown in Fig. 4. Using the drop of n_H in the zero temperature limit[21,25] we find that $B_{MI} = 10.1 \pm 0.2$ T (see Supplementary Note 5), which is well

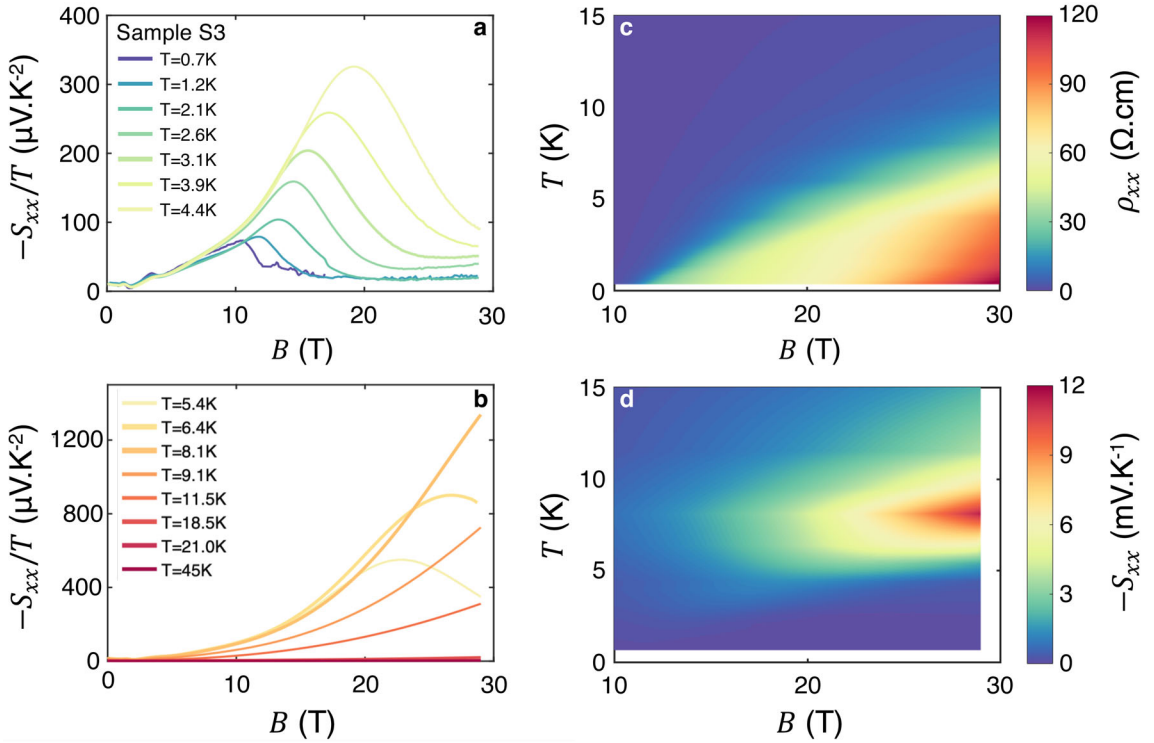

Fig. 3 High-field thermo-power and resistivity of InAs. a $-\frac{S_{xx}}{T}$ of sample S3 as a function of the magnetic field from $T = 0.7$ K to 4.4 K and **b** from $T = 5.4$ K to 45 K. **c** and **d** Temperature-magnetic field color map of the transverse resistivity ρ_{xx} and $-S_{xx}$ of sample S3.

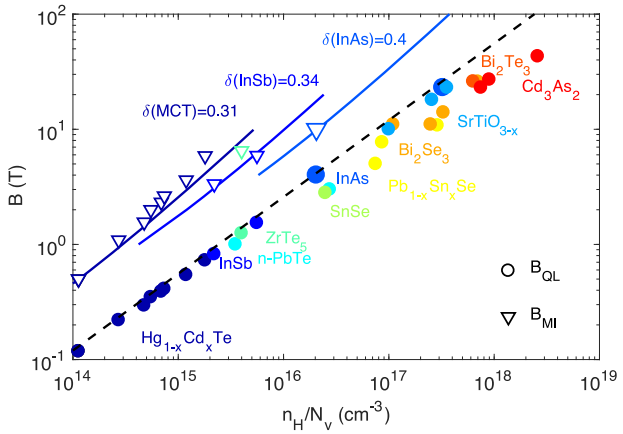

Fig. 4 Comparison of B_{QL} and B_{MI} in various doped semiconductors. Observed metal–insulator transition fields (taken as the drop in the Hall carrier density), B_{MI} (open triangles), and the positions of the last maximum in the resistivity or the Nernst effect, B_{QL} (filled circles) plotted as functions of the carrier densities of doped semiconductors. The points are extracted from references[7,21,40–50] (see Supplementary Note 5). The dashed-black line is the predicted $B_{QL} = \frac{\hbar(3\pi^2 n)^{\frac{2}{3}}}{e(1+|M|)}$ for an isotropic parabolic dispersion with the *g*-factor of InAs (g(InAs) = 15, $M = 0.13$). The solid curves represent the metal–insulator transition field vs. density calculated using Eq. (1) with $\delta = 0.31$($Hg_{0.8}Cd_2Te$), 0.34(InSb) and 0.4(InAs).

captured by Eq. (1) assuming a $\delta = 0.4$ as illustrated in Fig. 4. In the *k*-space this transition corresponds to a transfer of electrons from the LLL to a shallow band (formed by the localized electrons) located at an energy below the LLL[23].

Above $B = 15$ T, a novel regime is identified where ρ_{xx} varies almost linearly with the magnetic field and concomitant with a saturating $n_H \approx 10^{15}$ cm^{-3} and $\frac{S_{xx}}{T} = -21\mu$V K^{-2} at the lowest temperature. As a function of the temperature, ρ_{xx} first displays an activated behavior followed by a saturation at low temperature (see Supplementary Note 4). The deduced gap, Δ, is equal to 2 meV at $B = 30$ T and increases with the magnetic field up to $B = 50$ T (see Supplementary Note 4). As the temperature is increased, the transition shifts to higher magnetic field, becomes broader and vanishes above $T = 30$ K in the electrical response. Likewise, the peak in S_{xx} shifts to higher magnetic field. However, surprisingly, its amplitude increases. This striking observation is better appreciated by comparing the two color-maps of ρ_{xx} and S_{xx}, which are shown respectively in Fig. 3c, d. While ρ_{xx} is maximal at the lowest temperature, S_{xx} is maximal at around $T = 8$ K and that for all magnetic fields as shown in Fig. 5.a). At $B = 29$ T, $S_{xx}(T = 8\,\text{K})$ is as large as 11.3 mV K^{-1}, which is about 200 times larger than the zero-field thermopower and comparable with the "colossal" thermopower observed in ultra-low carrier density Ge ($n_H < 10^{13}$ cm^{-3}) where $S_{xx}(T = 10\,\text{K}) \approx 10-30$ mV K^{-1} (ref. [26]), in the strongly correlated semiconductors $FeSb_2$ ($n_H \approx 1 \times 10^{15}$ cm^{-3}) where $S_{xx}(T = 10\text{K}) \approx 10-30$ mV K^{-1} (refs. [27,28]) or in the fractional quantum Hall regime of 2DEGs where $S_{xx}(T = 5\,\text{K})$ reaches 50 mV K^{-1} (ref. [12]). Let us now discuss the origin of the two intriguing properties identified above B_{MI} : the saturating magnetoresistance and the giant Seebeck response.

DISCUSSION

The residual conductivity and carrier density at low temperature and high magnetic field contrasts with the insulating behavior of lightly doped InSb[21]. A key difference between both systems is the length scale of the fluctuations of the impurity potential. In highly doped semiconductors, large-scale fluctuations affect the density of state, in particular in its quantum limit regime[29]. Scanning tunneling microscopy (STM) measurements have revealed spatial fluctuations of the LLL in InAs on the energy scale of Γ = 3–4 meV, which result in a broadening of the shallow band and a tail in the

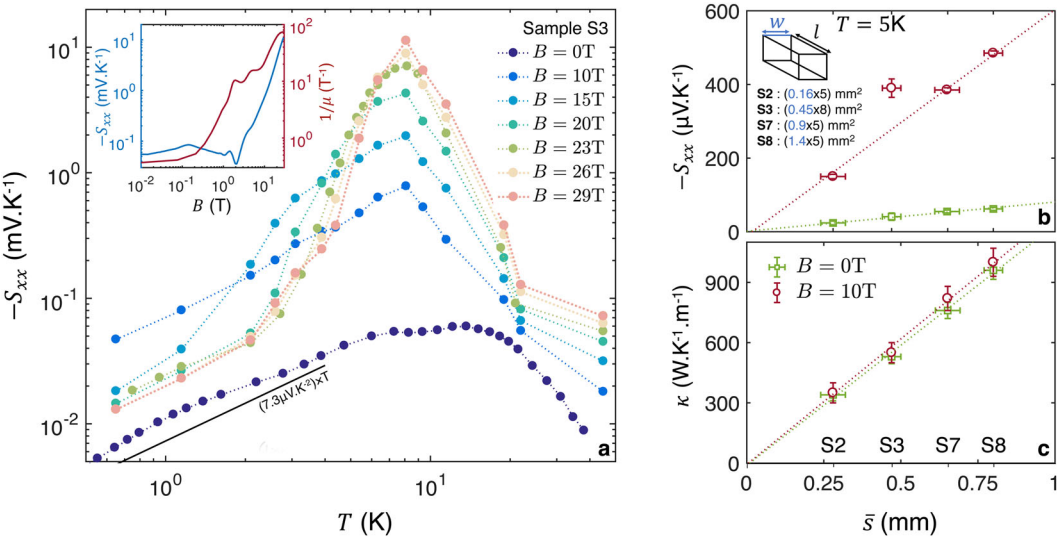

Fig. 5 Size dependence of S_{xx} and κ_{xx}. a $-S_{xx}$ (sample S3) as a function of temperature for various magnetic fields. The solid black line shows the thermopower value expected in the diffusive regime of a degenerate electron gas with $T_F = 100$ K. The inset shows a comparison of the field dependence of $-S_{xx}$ (left axis in blue) and $1/\mu_H$ (right axis in red) at $T = 8$ K. Both quantities are amplified by about a factor 200 between 0 T and 30 T. **b** $-S_{xx}$ function of the sample cross-section $\bar{s} = \sqrt{(\omega t)}$ (where ω and t are the sample width and thickness) at $T = 5$ K for $B = 0$T (in green open squares) and $B = 10$ T (in red open squares). For all the samples $t = 0.5$ mm and the value of ω is given in the inset. Both values are much shorter than the sample length, L. Error bars come from the error on the geometrical factor value of about 10%. **c** κ_{xx} function of $\bar{s}$ at $T = 5$ K for $B = 0$ T (green open circles) and $B = 10$ T (red open squares).

density of state of the LLL[30]. Such broadening manifests itself in the electrical transport properties by a gap (Δ) value much lower than the theoretical predictions[19] and a residual carrier concentration down to the lowest temperature well above B_{MI} as far as $\Gamma \approx \Delta$[29]. With a residual carrier density of $n_{H,B>B_{MI}} \approx 1\times10^{15}\,\mathrm{cm}^{-3}$ and a resistivity $\rho_{xx} \approx 100\,\Omega$.cm, these residual bulk electrons have a low mobility $\mu_{H,B>B_{MI}} = 60\,\mathrm{cm}^2\,\mathrm{V}^{-1}\,\mathrm{s}^{-1}$. Such poorly mobile carriers can be shunted by the conductance of the surface as it is the case of the magnetic freeze-out regime of $Hg_{1-x}Cd_xTe$[31,32]. Magneto-transport, magneto-optical[33,34] and angle-resolved photoemission spectroscopy measurements[35,36] on InAs have well documented the existence of an accumulation layer of carrier density $n_S = 1\times10^{12}\,\mathrm{cm}^{-2}$($E_F \approx 100$ meV) of mobility $\mu_{H,S} \approx 5000\,\mathrm{cm}^2\,\mathrm{V}^{-1}\,\mathrm{s}^{-1}$. For a sample thickness, e, the ratio of conductance from the bulk (σ_b) and the surface (σ_s) is given by: $\frac{\sigma_b}{\sigma_s} = \frac{en_{H,B>B_{MI}}\mu_{H,B>B_{MI}}}{n_S\mu_{H,s}}$. With the numbers given above, $\frac{\sigma_b}{\sigma_s} \approx 1$: both contributions are of the same order of magnitude. This is supported by the amplitude of the thermopower at low temperature for $B > B_{MI}$. In the presence of bulk and surface contributions, S_{xx} is given by the sum of the bulk and surface thermopower (labeled $S_{xx,B}$ and $S_{xx,S}$) balanced by their relative contribution to the total conductivity: $S_{xx} = \frac{\sigma_B S_{xx,B}+\sigma_S S_{xx,S}}{\sigma_B+\sigma_S}$. With a Fermi temperature of the surface states ($T_F \approx 900$ K[34]) much larger than the Fermi temperature of the residual bulk state ($T_{F,B>B_{MI}} = 18$K) $S_{xx,S} \ll S_{xx,B}$ with $\frac{S_{xx,B}}{T}$ expected to be $-46\,\mu\mathrm{V\,K}^{-2}$ in the diffusive regime of ionized-impurity scattering. With $\sigma_B \approx \sigma_S$, $\frac{S_{xx}}{T} \approx \frac{S_{xx,B}}{2T} = -23\,\mu\mathrm{V\,K}^{-2}$ in good agreement with the residual measured thermopower. Contributions from the surface states are further supported by the sample dependence of the low-temperature-high-field value of ρ_{xx} as discussed in Supplementary Note 4. Therefore, deep inside its quantum limit, the electrical transport properties of InAs reveal two types of contributions: a first from low mobility bulk electrons and a second from highly mobile electrons on the surface.

The field dependence of S_{xx} is qualitatively well captured by the Mott relation[37] ($\frac{S_{xx}}{T} = -\frac{\pi^2}{3}\frac{k_B^2}{e}\frac{\partial \ln(\sigma(\epsilon))}{\partial\epsilon}_{\epsilon=\epsilon_F}$): in the region where ρ_{xx} and ρ_{xy} (and thus σ_{xx}) vary the most with both the magnetic field and temperature that S_{xx} is the largest. As a function of the magnetic field, the increase happens close to B_{MI}, leading to a peak in the field dependence of S_{xx}. However, this relation fails to explain quantitatively the temperature evolution and the amplitude of the peak. As the temperature increases, the transition becomes broader and the amplitude of the peak is expected to vanish. In the activation regime σ_{xx} scales as $\exp(-\frac{\Delta}{k_BT})$ and S_{xx} as $\frac{k_B}{e}\frac{\Delta}{T}$. At $T = 8$ K and $B = 30$ T ($\Delta = 2$ meV), $S_{xx}(T = 8\,\mathrm{K})$ is at most $3\frac{k_B}{e} = 250\,\mu\mathrm{V\,K}^{-1}$ fifty times smaller than the measured value. Therefore, another source of entropy has to be invoked such as the phonon bath.

At zero magnetic field the phonon-drag effect is known to enhance the thermoelectrical response of low-doped semiconductors. The phonon drag picture conceived by Herring[14] quantifies the additional contribution to the Peltier coefficient, Π, by the thermal current carried by phonons. The Peltier coefficient, which is the ratio of heat current to charge current, is linked to the Seebeck coefficient through the Kelvin relation. According to Herring, the phonon drag contribution to the Peltier coefficient is:

$$\Pi_{ph} = \pm\Lambda m^* v_s^2 \frac{\tau_{ph}}{\tau_e} \quad (2)$$

Here, $\Lambda < 1$ quantifies the momentum exchange rate between phonons and electrons[14], τ_{ph} and τ_e are the phonon and electron scattering rates, m^* is the effective mass of the electron and v_{ph} is the sound velocity. One can see that phonon drag requires a finite Λ and is boosted by a large $\frac{\tau_{ph}}{\tau_e}$ and/or a large effective mass (like in $FeSb_2$[28]). Using the Kelvin relation, Eq. (2) leads to:

$$S_{ph} = \pm\frac{k_B}{e}\Lambda\frac{m^* v_{ph}^2}{k_BT}\frac{\tau_{ph}}{\tau_e} = \pm\Lambda\frac{\ell_{ph}v_{ph}}{\mu_H T} \quad (3)$$

Thus, a large Seebeck response in units of $\frac{k_B}{e}$ is possible thanks to phonon drag. It requires $\tau_{ph} \gg \tau_e$ and a finite Λ. Herring showed that in intrinsic semiconductors, such as Si and Ge, the large $\frac{\tau_{ph}}{\tau_e}$ ratio provides a key to understand the large magnitude of the Seebeck response at cryogenic temperatures[38,39].

Let us discuss how the magnetic field squeezes τ_e, leaves τ_{ph} unaffected and thus boosts their ratio. In contrast to the diffusive response, S_{ph} scales with the sample dimensions, the inverse of the mobility and can exceed by far $\frac{k_B}{e}$. A crucial test of Eq. (3) comes from the size and mobility dependence of S_{xx}. As shown in Fig. 5b, c, both S_{xx} and κ_{xx} are size-dependent and scale with the cross-section of the sample, $\bar{s}$, as expected for phonons in the ballistic regime for samples where $\bar{s} \ll L$ where L is the sample length. The slope of κ_{xx} vs. $\bar{s}$ is, however, independent of the magnetic field (since it only depends on l_{ph}), while the slope of S_{xx} vs. $\bar{s}$ increases with increasing magnetic field due to the reduction of μ_H. As expected from Eq. (3) and illustrated in the inset of Fig. 5a), the changes induced by the magnetic field in $-S_{xx}$ and in μ_H^{-1} are comparable. At $T = 8$ K, between $B = 0$ T and $B = 29$ T, $-S_{xx}(T = 8\,\mathrm{K})$ is amplified by a factor of 202 and μ_H decreases by a factor of 196. Using Eq. (3) at high magnetic field, we find that $\Lambda \ll 1$. This is not a surprise, given the temperature dependence of ρ_{xx}, which shows that below $T = 100$ K, electrons are mostly scattered by ionized impurities and not by phonons.

The phonon drag picture, therefore, provides a quantitative explanation of the giant field-induced Seebeck effect in InAs. We note that below $T = 8$ K, S_{xx} peaks in magnetic field while S_{ph} is expected to be the largest at the highest magnetic field (where μ_H is the lowest). This implies either a shunt of S_{ph} by the relatively small thermoelectrical response of the surface states or a more elaborate bulk phonon drag picture that would be maximum close to B_{MI}, where the bulk shallow band is partially filled as it has been proposed in $FeSb_2$[27]. Interestingly $FeSb_2$ and InAs above B_{MI} share in common the same activation gap (of the order of a few meV), the same carrier density (10^{15} cm^{-3}) and the presence of bulk in-gap states. However, with resistivity values two orders of magnitude larger in InAs than in $FeSb_2$, the power factor of InAs is only 10 μW K^{-2} cm^{-1} (two orders of magnitude smaller than in $FeSb_2$).

While a purely electronic mechanism has been recently proposed to give rise to an unbounded thermopower in Dirac/Weyl semimetals in their quantum limit regime[13], our results show that the phonon drag effect is another road to boost the diffusive response of low carrier density metals across their field-induced MIT. Up to now, this transition has been studied only in a limited number of cases and the thermoelectric properties of dilute metals remain vastly unexplored. As illustrated in Fig. 4, a large class of materials (ranging from well-known doped semiconductors to new topological materials) remains to be studied, in particular at higher doping (and, therefore, at high magnetic field) where larger Λ can be attained, favoring even larger S_{ph}.

METHODS

Samples and measurements description

The InAs samples were cleaved into rectangular plates (with typical dimensions $[1 \times 5 - 10 \times 0.5]$mm^3) from a wafer of nominal carrier densities of $n(W_1) \approx 2 \times 10^{16}$ cm^{-3} bought from Wafer Technology Ltd (www.wafertech.co.uk). The samples were etched in a HCl-methanol solution prior to any experiment. Electrical contacts were made with silver paste. The electrical and heat currents were applied along the [0 −1 1] direction and the magnetic field along the [0 0 1] direction. DC-electrical and thermoelectrical transport measurements were done in a Quantum Design PPMS using a home built stick up to 14 T, in a dilution fridge up to $B = 17$ T, an ^{3}He cryostat up to $B = 35$ T at both LNCMI-Grenoble and HMFL (Nijmegen). These measurements were completed by electrical transport measurements up to $B = 56$ T between $T = 1.4$ K and $T = 30$ K. For further experimental details see supplemental material details on the electronic properties, the Landau levels spectrum, the field dependence of the gap, and the sample dependence in the ultra-quantum limit regime of our InAs samples.

DATA AVAILABILITY

All data supporting the findings of this study are available from the corresponding authors A.J. and B.F. upon request.

Received: 14 August 2020; Accepted: 12 November 2020;
Published online: 15 December 2020

REFERENCES

1. Nolas, G. S., Sharp, J. & Goldsmid, J. *Thermoelectrics: Basic Principles and New Materials Developments*, Vol. 45 (Springer Science & Business Media, 2013).
2. Behnia, K. *Fundamentals of Thermoelectricity*. (Oxford University Press, Oxford, 2015).
3. Behnia, K., Méasson, M.-A. & Kopelevich, Y. Oscillating Nernst-Ettingshausen effect in bismuth across the quantum limit. *Phys. Rev. Lett.* **98**, 166602 (2007).
4. Zhu, Z., Yang, H., Fauqué, B., Kopelevich, Y. & Behnia, K. Nernst effect and dimensionality in the quantum limit. *Nat. Phys.* **6**, 26–29 (2010).
5. Zhu, Z., Fauqué, B., Fuseya, Y. & Behnia, K. Angle-resolved Landau spectrum of electrons and holes in bismuth. *Phys. Rev. B* **84**, 115137 (2011).
6. Tieke, B. et al. Magnetothermoelectric properties of the degenerate semiconductor HgSe: Fe. *Phys. Rev. B* **54**, 10565–10574 (1996).
7. Liang, T. et al. Evidence for massive bulk Dirac fermions in $Pb_{1-x}Sn_xSe$ from Nernst and thermopower experiments. *Nat. Commun.* **4**, 2696 (2013).
8. Zhang, W. et al. Observation of a thermoelectric Hall plateau in the extreme quantum limit. *Nat. Commun.* **11**, 1046 (2020).
9. Puri, S. M. & Geballe, T. H. Phonon drag in *n*-type InSb. *Phys. Rev.* **136**, 1767–1774 (1964).
10. Fauqué, B. et al. Magnetothermoelectric properties of Bi_2Se_3. *Phys. Rev. B* **87**, 035133 (2013).
11. Han, F. et al. Quantized thermoelectric Hall effect induces giant power factor in a topological semimetal. *Nat. Comm.* **11**, 6167 (2020). https://www.nature.com/articles/s41467-020-19850-2.
12. Fletcher, R., Maan, J. C., Ploog, K. & Weimann, G. Thermoelectric properties of GaAs–$Ga_{1-x}Al_xAs$ heterojunctions at high magnetic fields. *Phys. Rev. B* **33**, 7122–7133 (1986).
13. Skinner, B. & Fu, L. Large, nonsaturating thermopower in a quantizing magnetic field. *Sci. Adv.* **4**, eaat2621 (2018).
14. Herring, C. Theory of the thermoelectric power of semiconductors. *Phys. Rev.* **96**, 1163–1187 (1954).
15. Jay-Gerin, J. P. Thermoelectric power of semiconductors in the extreme quantum limit. II. the "phonon-drag" contribution. *Phys. Rev. B* **12**, 1418–1431 (1975).
16. Rode, D. L. Electron transport in InSb, InAs, and InP. *Phys. Rev. B* **3**, 3287–3299 (1971).
17. Cetas, T. C., Tilford, C. R. & Swenson, C. A. Specific heats of Cu, GaAs, GaSb, InAs, and InSb from 1 to 30K. *Phys. Rev.* **174**, 835–844 (1968).
18. Le Guillou, G. & Albany, H. J. Phonon conductivity of InAs. *Phys. Rev. B* **5**, 2301–2308 (1972).
19. Kaufman, L. A. & Neuringer, L. J. Magnetic freezeout and band tailing in n-InAs. *Phys. Rev. B* **2**, 1840–1846 (1970).
20. Kadri, A., Aulombard, R., Zitouni, K., Baj, M. & Konczewicz, L. High-magnetic-field and high-hydrostatic-pressure investigation of hydrogenic-and resonant-impurity states in n-type indium arsenide. *Phys. Rev. B* **31**, 8013–8023 (1985).
21. Shayegan, M., Goldman, V. J. & Drew, H. D. Magnetic-field-induced localization in narrow-gap semiconductors $Hg_{1-x}Cd_xTe$ and InSb. *Phys. Rev. B* **38**, 5585–5602 (1988).
22. Aronzon, B. A. & Tsidilkovskii, I. M. Magnetic-field-induced localization of electrons in fluctuation potential wells of impurities. *Phys. Status Solidi (b)* **157**, 17–59 (1990).
23. Yafet, Y., Keyes, R. & Adams, E. Hydrogen atom in a strong magnetic field. *J. Phys. Chem. Solids* **1**, 137 – 142 (1956).
24. Shklovskii, B. I. & Efros, A. L. *Electronic Properties of Doped Semiconductors*. (Springer-Verlag, New York, 1984).
25. Rosenbaum, T. F., Field, S. B., Nelson, D. A. & Littlewood, P. B. Magnetic-field-induced localization transition in HgCdTe. *Phys. Rev. Lett.* **54**, 241–244 (1985).
26. Inyushkin, A. V., Taldenkov, A. N., Ozhogin, V. I., Itoh, K. M. & Haller, E. E. Isotope effect on the phonon-drag component of the thermoelectric power of germanium. *Phys. Rev. B* **68**, 153203 (2003).
27. Bentien, A., Johnsen, S., Madsen, G. K. H., Iversen, B. B. & Steglich, F. Colossal Seebeck coefficient in strongly correlated semiconductor $FeSb_2$. *Europhys. Lett. (EPL)* **80**, 17008 (2007).
28. Takahashi, H. et al. Colossal Seebeck effect enhanced by quasi-ballistic phonons dragging massive electrons in $FeSb_2$. *Nat. Commun.* **7**, 12732 (2016).
29. Dyakonov, M., Efros, A. & Mitchell, D. Magnetic freeze-out of electrons in extrinsic semiconductors. *Phys. Rev.* **180**, 813–818 (1969).
30. Morgenstern, M., Wittneven, C., Dombrowski, R. & Wiesendanger, R. Spatial fluctuations of the density of states in magnetic fields observed with scanning tunneling spectroscopy. *Phys. Rev. Lett.* **84**, 5588–5591 (2000).
31. Mullin, J. B. & Royle, A. Surface oxidation and anomalous electrical behaviour of cadmium mercury telluride. *J. Phys. D: Appl. Phys.* **17**, L69–L72 (1984).

32. Antcliffe, G. A., Bate, R. T. & Reynolds, R. A. Oscillatory magnetoresistance from a n-type inversion layer with nonparabolic bands. *The Physics of Semi-metals and Narrow Gap Semi-conductors: Proceedings*. 499–509 (Pergamon, 1970).
33. Tsui, D. C. Observation of surface bound state and two-dimensional energy band by electron tunneling. *Phys. Rev. Lett.* **24**, 303–306 (1970).
34. Reisinger, H., Schaber, H. & Doezema, R. E. Magnetoconductance study of accumulation layers on *n*−InAs. *Phys. Rev. B* **24**, 5960–5969 (1981).
35. Olsson, L. O. et al. Charge accumulation at InAs surfaces. *Phys. Rev. Lett.* **76**, 3626–3629 (1996).
36. King, P. D. C. et al. Surface band-gap narrowing in quantized electron accumulation layers. *Phys. Rev. Lett.* **104**, 256803 (2010).
37. Ziman, J. M. *Principle oF the Theory of Solids* (Cambridge University Press, 1972).
38. Geballe, T. H. & Hull, G. W. Seebeck effect in germanium. *Phys. Rev.* **94**, 1134–1140 (1954).
39. Geballe, T. H. & Hull, G. W. Seebeck effect in silicon. *Phys. Rev.* **98**, 940–947 (1955).
40. Oswald, J., Goldberg, B. B., Bauer, G. & Stiles, P. J. Magnetotransport studies on the metallic side of the metal-insulator transition in PbTe. *Phys. Rev. B* **40**, 3032–3039 (1989).
41. Bhattacharya, A., Skinner, B., Khalsa, G. & Suslov, A. V. Spatially inhomogeneous electron state deep in the extreme quantum limit of strontium titanate. *Nat. Commun.* **7**, 12974 (2016).
42. Assaf, B. A. et al. Negative longitudinal magnetoresistance from the anomalous N = 0Landau level in topological materials. *Phys. Rev. Lett.* **119**, 106602 (2017).
43. Wang, Z. et al. Defects controlled hole doping and multivalley transport in SnSe single crystals. *Nat. Commun.* **9**, 47 (2018).
44. Köhler, H. & Wöchner, E. The g-factor of the conduction electrons in Bi_2Se_3. *Phys. Status Solidi (b)* **67**, 665–675 (1975).
45. Analytis, J. G. et al. Two-dimensional surface state in the quantum limit of a topological insulator. *Nat. Phys.* **6**, 960–964 (2010).
46. Rischau, C. W. *Irradiation-induced doping of Bismuth Telluride Bi_2Te_3* (Ecole Polytechnique, Université Paris Saclay, 2010).
47. Tang, F. et al. Three-dimensional quantum Hall effect and metal-insulator transition in $ZrTe_5$. *Nature* **569**, 537–541 (2019).
48. Xiang, Z. J. et al. Angular-dependent phase factor of Shubnikov-de Haas oscillations in the Dirac semimetal Cd_3As_2. *Phys. Rev. Lett.* **115**, 226401 (2015).
49. Narayanan, A. et al. Linear magnetoresistance caused by mobility fluctuations in *n*-doped Cd_3As_2. *Phys. Rev. Lett.* **114**, 117201 (2015).
50. Zhao, Y. et al. Anisotropic Fermi surface and quantum limit transport in high mobility three-dimensional Dirac semimetal Cd_3As_2. *Phys. Rev. X* **5**, 031037 (2015).

ACKNOWLEDGEMENTS

We thank A. Akrap, R. Daou, B. Skinner, and J. Tomczak for useful discussions. This work is supported by JEIP-Collège de France, by the Agence Nationale de la Recherche (ANR-18-CE92-0020-01, ANR-19-CE30-0014-04) and by a grant attributed by the Ile de France regional council. Part of this work was performed at LNCMI-CNRS and HFML-RU/NWO-I, members of the European Magnetic Field Laboratory (EMFL).

AUTHOR CONTRIBUTIONS

A.J. and B.F. conducted the electrical, thermoelectrical, and thermal conductivity measurements up to $B = 17$ T. High-field measurements have been conducted by A.J., G.S., B.F. at LNCMI-Grenoble, by A.J., C.W.R., S.W. at HFML and by C.W.R., S.B., and C.P. at LNCMI-Toulouse. A.J. and B.F. analyzed the data. A.J., K.B., and B.F. wrote the manuscript.

COMPETING INTERESTS

The authors declare no competing interests.

ADDITIONAL INFORMATION

Supplementary information is available for this paper at https://doi.org/10.1038/s41535-020-00296-0.

Correspondence and requests for materials should be addressed to A.J. or B.F.

Reprints and permission information is available at http://www.nature.com/reprints

Publisher's note Springer Nature remains neutral with regard to jurisdictional claims in published maps and institutional affiliations.